Available online at www.sciencedirect.com
SCIENCE DIRECT®
Journal of Catalysis 224 (2004) 156–163
JOURNAL OF CATALYSIS
www.elsevier.com/locate/jcat

Grafting TiO_2 on MCM-41 as a TiO_2 support for vanadia for catalytic oxidation of ethanol—EXAFS and XANES analyses of vanadium

Hsiu-Mei Lin,[a] Sheng-Tsang Kao,[a,b] Kuo-Min Lin,[c] Jen-Ray Chang,[c,*] and Shin-Guang Shyu [a,b,*]

[a] *Institute of Chemistry, Academia Sinica, Nankan, Taipei, Taiwan, ROC*
[b] *Department of Chemistry, National Central University, Chungli, Taiwan, ROC*
[c] *Department of Chemical Engineering, National Chung Cheng University, Chia-Yi, Taiwan, ROC*

Received 26 November 2003; revised 22 January 2004; accepted 9 February 2004

Abstract

Titanium oxide was grafted on the surface of MCM-41 to produce a mesoporous TiO_2/MCM-41 composite to serve as a catalyst support. Vanadia was grafted on this titania support to produce V_2O_5/TiO_2/MCM-41 and catalytic oxidation of ethanol by air was used as a probe reaction to study the influence of the support on the catalytic behavior of this catalyst. Catalyst V_2O_5/TiO_2/MCM-41 has reactivity five times higher than the reactivity of vanadia on MCM-41. EXAFS analysis of vanadium indicates that vanadia on both supports have similar structures and polymeric morphologies. The enhancement of reactivity was due to the direct dispersion of vanadia on TiO_2 in V_2O_5/TiO_2/MCM-41 as indicated by the EXAFS and XANES studies. This TiO_2-grafted MCM-41 mesoporous framework thus has high potential for use as a mesoporous TiO_2 support. Such support is superior to traditional anatase TiO_2, pure mesoporous TiO_2, or TiO_2/SiO_2 supports owing to its much larger surface area and better thermal stability at elevated temperatures.

Keywords: Mesoporous; EXAFS; XANES; Vanadia; Titania; Catalyst

1. Introduction

Anatase titania-supported vanadium oxide catalysts are widely used in the industry for selective catalytic reduction of NO_x, catalytic oxidation reactions, and ammoxidation of picolines [1]. However, commercial anatase titania normally has low surface area and low mechanical strength, and it sinters more easily than silica and alumina supports. Considerable efforts have recently been made on applying mixed titania–silica [2] or titania–alumina [3] as a titania support for vanadia-based catalysts to overcome these drawbacks. Nevertheless, a high surface area titania support used for vanadia-based catalysts has not been reported so far.

Recent developments of mesoporous materials initiated the preparation of mesoporous TiO_2 with the possibility of producing high surface area TiO_2 [4–6]. However, high surface area mesoporous TiO_2 tends to collapse at high temperatures or contains phosphorous, which results in limiting its usage as a catalyst support [7–10]. Grafting TiO_2 on MCM-41 has provided a mesoporous framework with a catalytically active TiO_2 surface [11]. In addition, TiO_2-grafted MCM-48 was reported to maintain the mesoporous structure with a high surface area up to 1073 K [12]. Herein we report a vanadium-based catalyst with a TiO_2-grafted MCM-41 as the support. This catalyst (V_2O_5/TiO_2/MCM-41) has a high surface area with uniform pore size. Catalytic oxidation reactions of ethanol with air are used as probe reactions to demonstrate the role of TiO_2 in improving catalytic performance of the resultant catalyst. EXAFS (extended X-ray absorption fine structure) and XANES (X-ray absorption near-edge structure) spectroscopies were used to characterize the structures of vanadium on both MCM-41 and TiO_2/MCM-41.

2. Experimental

2.1. General procedures

All reactions and other manipulations were performed by use of standard Schlenk techniques under an atmosphere

* Corresponding authors. Fax: +886-2-27831237.
E-mail addresses: chmjrc@ccunix.ccu.edu.tw (J.-R. Chang), sgshyu@chem.sinica.edu.tw (S.-G. Shyu).

0021-9517/$ – see front matter
doi:10.1016/j.jcat.2004.02.023

of nitrogen. Commercially available chemicals were purchased and used without further purification. Cetyltrimethylammonium bromide (CTAB), vanadium oxytripropoxide ($VO(OC_3H_7)_3$), and titanium isopropoxide ($Ti(OCH(CH_3)_2)_4$) were purchased from Acros, and Silica Fumed (SiO_2) was from Sigma. All solvents were dried with Na and benzophenon under N_2 and distilled immediately prior to use. BET surface area measurements were recorded on a ASAP 2010. Powder X-ray spectra were recorded on a Siemens D5000 powder X-ray spectrometer. Energy-dispersive spectra (EDS) were recorded on a scanning electron microscope (JSM-5400) equipped for an energy-dispersive X-ray spectrometer (eXL, Link Systems). ICP-MS spectra were recorded on a Perkin–Elmer SCIEX ELAN 5000 spectrometer at the National Hsing Hwa University.

2.2. Preparation of MCM-41

A solution of 5.10 ml (5.18 g, 0.014 mol, 25% w/w aq soln) tetramethylammonium hydroxide was added slowly into a solution of cetyltrimethylammonium bromide (7.38 g, 0.02 mol) in 50.0 ml deionized water in a Teflon reactor at room temperature. After stirring the mixture for 30 min, a clear solution was obtained. Silica Fumed (4.50 g, 0.075 mol) was then slowly added into the above solution. After the mixture was stirred for 2 h, it was allowed to stand for 24 h. The mixture was then heated at 423 K for 48 h in a hydrothermal bomb. The slurry was washed with deionized water and dried in an oven at 333 K. The resulting white powder was calcined at 823 K under air. The white MCM-41 was characterized by powder X-ray diffraction spectra.

2.3. Preparation of V_2O_5/MCM-41

MCM-41 (1.67 g) was dried in an oven at 393 K for 24 h in order to remove the water. The dried MCM-41 was then placed in a side-arm flask under nitrogen and 25.0 ml of hexane was added into the flask. Vanadium oxytripropoxide (0.30 ml, 1.28 mmol) was added to the above mixture which was then stirred overnight. After filtration and washing with hexane to remove the excess vanadium oxytripropoxide, the mixture was dried in an oven at 333 K. The resulting yellow powder was calcined at 723 K for 8 h under air. The yellow product V_2O_5/MCM-41 was characterized by powder X-ray diffraction spectra, EDS, and ICP-MS.

2.4. Preparation of TiO_2/MCM-41

Preparation conditions similar to those for V_2O_5/MCM-41 were applied to prepare TiO_2/MCM-41. MCM-41 (1.67 g) and 4.20 ml (4.00 g, 14.04 mmol) of titanium isopropoxide were used. The white product TiO_2/MCM-41 was characterized by powder X-ray diffraction and EDS.

2.5. Preparation of V_2O_5/TiO_2/MCM-41

Preparation conditions similar to those for V_2O_5/MCM-41 were applied to prepare V_2O_5/TiO_2/MCM-41. The amounts 2.00 g of TiO_2/MCM-41 and 0.36 ml (0.37 g, 1.54 mmol) of vanadium oxytripropoxide were used in the preparation. The yellow product V_2O_5/TiO_2/MCM-41 was characterized by powder X-ray diffraction spectra, EDS, and ICP-MS.

2.6. Ethanol oxidation studies

The catalysts were tested in a flow system having a fixed-bed reactor with an inside diameter of 1.2 cm and volume of 94.0 ml. The reactor was heated electrically and temperature-controlled by a PID temperature controller with a sensor at the outer wall of the reactor. The reaction temperature was monitored and controlled using a sensor located at the center of the catalyst bed. The temperature difference between the outer reactor wall and the center of the catalyst bed was about 10 K. Reaction products were trapped using a condenser at 268 K. Both liquid and gaseous products were analyzed using a gas chromatography, Shimadzu Model GC 14-B equipped with a DB-WAX capillary column of 30 m × 0.321 mm i.d. (J&W Scientific).

The reactor was packed with 1.0 g catalyst of particle size 500–1000 μm mixed with inert SiO_2 (Merck) in a ratio of 1:20 by volume. A gradient packing method was used so that the catalyst bed would have a nearly uniform temperature and the wall and bypassing effects would be minimized. Ethanol (Aldrich, 99.5 vol%) feed and air at the desired rates were metered into the reaction system using mass-flow controllers. Upon mixing, the mixtures flow downward through the reactor to carry out the reactions at the desired temperature and pressure. The reactor effluent was cooled and recovered for analyses. Based on the material balances of test results, performance parameters such as conversion, selectivity, purity, and "composition products" were calculated.

2.7. X-ray absorption spectroscopy (XAS)

All X-ray absorption spectra of the V K-edge (5465 eV) and Ti K-edge (4966 eV) were measured on the beam line BL17C at the Synchrotron Radiation Research Center (SRRC) in Hsinchu, Taiwan, with a storage ring energy 1.5 GeV and a beam current between 120 and 200 mA. The EXAFS measurements were performed in transmission mode at the X-ray Wiggler beam line with a double-crystal Si(111) monochromator. The higher X-ray harmonics were minimized by detuning the double-crystal monochromator to 80% of the maximum. The ion chambers used for measuring the incident (I_0) and transmitted (I) synchrotron beam intensities were filled with a mixture of N_2 and He gases and a pure N_2 gas, respectively. Moreover, to ensure reliability of the spectra, the spectra of V metal foil and Ti metal

foil were also monitored to evaluate the stability of the energy scale for each measurement. XANES of Ti spectra were initially acquired at room temperature in a He purge and after heating to 723 K in O_2/He (20/80), holding for 30 min at 723 K.

Data reduction and data analysis were performed with the XDAP code developed by Vaarkamp et al. [13]. Standard procedures were used to extract the EXAFS data from the measured absorption spectra. The preedge was approximated by a modified Victoreen curve [14] and the background was subtracted using cubic spline routines [15,16]. Normalization was performed by dividing the data by the height of the absorption edge at 50 eV above the edge [14]. Phase shifts and backscattering amplitudes functions of V–V, V–Ti, and V–O were used as reference files to analyze the EXAFS data. The reference functions of V–V and V–Ti are generated by FEFF7 code [17] and V–O is extracted from the EXAFS function of the V_2O_5 compound.

Data analysis was performed by multiple shell fitting in R space ($1 < R < 4.0$ Å, $3.5 < k < 13$ Å^{-1}, k-weighting 3). The structure model of V_2O_5/TiO_2/MCM-41 is similar to that proposed by Gao et al. [18], whereas each backscatter atom was identified by a difference-file technique with phase-corrected Fourier transformations. The final fit parameters were obtained after a full optimization of all parameters in k^3 weighting in the Fourier transformations.

3. Results and discussion

3.1. Preparation and characterization of V_2O_5/TiO_2/MCM-41

MCM-41 was prepared by hydrothermal treatment of SiO_2 and C_{16}TABr [19]. It has a mesoporous structure with 1479 m^2/g BET surface area, 27.0 Å uniform pore size, and 40.2 Å d(100) spacing in its powder X-ray spectrum (Fig. 1). This MCM-41 was further grafted with $Ti(OC_3H_7)_4$ under an inert environment to produce titanium-grafted MCM-41 (TiO_2/MCM-41) [12].

The surface of MCM-41 contains silanol Si–OH groups which can react with metal alkoxy groups to produce M–O–Si linkages with the elimination of alcohols. The MCM-41 should be dried before the grafting procedure in order to remove absorbed water on its surface such that hydrolysis of metal alkoxide in the latter grafting step can be avoided. In addition, the grafting reaction should be carried out under an inert environment to avoid the hydrolysis of metal alkoxide. Under such conditions, around 20 wt% of TiO_2 (15 at.% of Ti) can be grafted on the surface of MCM-41 under an excess amount of $Ti(OC_3H_7)_4$. Calcined TiO_2/MCM-41 (at 723 K) preserves the mesoporous structure with 1237 m^2/g BET surface area, 26.0 Å uniform pore size, and 40.7 Å d(100) spacing in its powder X-ray spectrum (Fig. 1). Energy-dispersive spectroscopy of TiO_2/MCM-41 clearly indicates the presence of titanium. This TiO_2/MCM-41 can maintain its mesoporous structure up to 1073 K. The composition analysis, d spacing, pore size, and surface area of the catalysts are listed in Table 1.

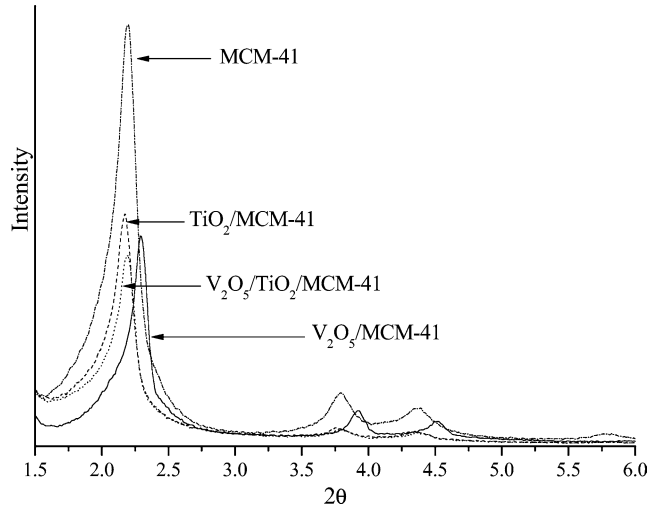

Fig. 1. Powder X-ray spectrum of MCM-41, V_2O_5/TiO_2/MCM-41, V_2O_5/TiO_2/MCM-41, and V_2O_5/MCM-41.

Vanadia was then grafted onto this TiO_2/MCM-41 by using $VO(OCH_2CH_2CH_3)_3$ [20] as a grafting reagent to obtain the supported vanadia catalyst (V_2O_5/TiO_2/MCM-41). Similarly, the TiO_2/MCM-41 was dried before the grafting step and the grafting reaction was carried out under an inert environment to avoid water. An excess amount of $VO(OCH_2CH_2CH_3)_3$ was used and around 14 wt% of V_2O_5 (11 at.% of V) was grafted on the supports. The resultant

Table 1
Composition, d(100) spacing, pore size, pore volume, and surface area of MCM-41, TiO_2/MCM-41, V_2O_5/TiO_2/MCM-41, and V_2O_5/MCM-41

Catalyst	V_2O_5 wt% (V mol%)	TiO_2 wt% (Ti mol%)	SiO_2 wt% (Si mol%)	d(100) spacing (Å)	Pore size (Å)	Pore volume (cm^3/g)	BET surface area (m^2/g)
MCM-41	–	–	–	40.43	27	1.00	1489
TiO_2/MCM-41	–	19.5 (15.4)	80.5 (84.6)	40.73	26	0.59	1237
V_2O_5/MCM-41	14.6 (11.8)	–	85.4 (88.2)	40.66	26	0.66	953
V_2O_5/TiO_2/MCM-41	12.9 (9.3)	17.6 (14.5)	69.5 (76.2)	40.45	25.5	0.41	713

Table 2
Product distribution in conversion of ethanol catalyzed by V_2O_5/TiO_2/MCM-41 and V_2O_5/MCM-41

	Catalyst[a]					
Product (wt%)	V_2O_5/TiO_2/MCM-41 383 K	V_2O_5/MCM-41 383 K	V_2O_5/TiO_2/MCM-41 428 K	V_2O_5/MCM-41 428 K	V_2O_5/TiO_2/MCM-41 458 K	V_2O_5/MCM-41 458 K
Acetaldehyde	0.732	0.466	0.692	0.458	0.512	0.302
Ethyl acetate	0.236	0.293	0.250	0.295	0.333	0.300
Acetic acid	0.002	0.196	0.002	0.120	0.040	0.004
Carbon dioxide	0.022	0.035	0.045	0.110	0.098	0.372
Other species[b]	0.008	0.010	0.011	0.017	0.017	0.022

[a] Pressure = 5 atm, WHSV (weight hourly space velocity) = 2.5 h^{-1}, air/ethanol = 7.6.
[b] Other species include formic acid, paraldehyde, ethyl formate.

calcined V_2O_5/TiO_2/MCM-41 catalyst (at 723 K) retains 713 m^2/g BET surface area, 25.5 Å uniform pore size, and 40.5 Å $d(100)$ spacing in its powder X-ray spectrum (Fig. 1). In comparison, vanadia was also grafted onto MCM-41 with a similar dose of vanadia per unit weight of the catalyst as that of TiO_2/MCM-41 support. EDS spectra of both catalysts V_2O_5/TiO_2/MCM-41 and V_2O_5/MCM-41 confirm the presence of vanadium. The resultant calcined V_2O_5/MCM-41 catalyst (at 723 K) has a BET surface area of 953 m^2/g with 26.0 Å uniform pore size, and 40.7 Å $d(100)$ spacing in its powder X-ray spectrum (Fig. 1).

The MCM-41 and TiO_2/MCM-41-supported vanadia catalysts used in the experiments were intended to provide similar amounts of vanadia. Although excess grafting reagent was used, similar amounts of vanadia were grafted on both supports (Table 1). The surface areas of V_2O_5/MCM-41 and V_2O_5/TiO_2/MCM-41 are less than the parent MCM-41. This is because the pore size slightly decreased after the grafting and the additional weight of the grafting materials (vanadia, titania, or both) increases the weight per unit volume of the mesoporous materials.

3.2. Ethanol oxidation studies

It has been reported that titania–silica (TiO_2/SiO_2) is a better support than SiO_2 for vanadia-based catalysts in the catalytic oxidation of alcohol with air [21,22]. In order to evaluate whether the TiO_2/MCM-41 can be used as a TiO_2 support like titania–silica, ethanol oxidation was applied to test the catalytic behavior of V_2O_5/MCM-41 and V_2O_5/TiO_2/MCM-41. The reaction is carried out in a fixed-bed reactor under five atmospheres of air. The WHSV (weight hourly space velocity) is 2.5 h^{-1} and air/ethanol is 7.6. The conversion rates of both catalysts are shown in Fig. 2. The selectivity is shown in Table 2.

As shown from the results of oxidation (Fig. 2), the ethanol conversion of the oxidation reaction catalyzed by V_2O_5/TiO_2/MCM-41 was higher than that by V_2O_5/MCM-41 up to fivefold at low temperatures. This suggests that the V_2O_5/TiO_2/MCM-41 catalyst has higher reactivity than V_2O_5/MCM-41 for each unit surface area in the catalytic reaction. In addition, as shown in Table 2, the percentage amount of the main product (acetaldehyde and ethyl acetate)

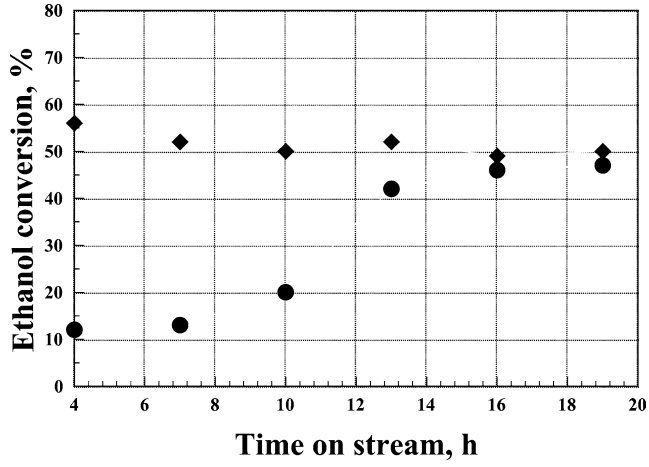

Fig. 2. Total conversion of ethanol catalyzed by (●) V_2O_5/MCM-41; (◆) V_2O_5/TiO_2/MCM-41 (operating conditions: initial temperature = 383 K, ramping temperature = 5 K/h, pressure = 5 atm, WHSV (weight hourly space velocity) = 2.5 h^{-1}; air/ethanol = 7.6).

is higher for V_2O_5/TiO_2/MCM-41 than for V_2O_5/MCM-41 at both low temperature (383 K) and high temperature (458 K). These observations imply that the resultant TiO_2/MCM-41 is a better support than MCM-41. This is consistent with the reported enhancement of vanadia reactivity on TiO_2/SiO_2 than SiO_2 in the catalytic ethanol oxidation [21,22].

Assuming that the ethanol oxidation reaction is catalyzed by vanadium oxide and the reaction occurs through a rate-determining surface reaction, the rate constant for the reaction will be composed of two terms, k_s (surface reaction rate constant) and the K_{EtOH} (adsorption constant of ethanol). Thus, apparent activation energy can be formulated by $E_{app} = E_s$ (activation energy of surface reaction) + H_a (adsorption heat of ethanol). Since the enthalpy of adsorption is negative, the apparent energy can be either positive or negative, depending on the magnitude of E_s and H_a.

By defining the turnover frequency (TOF) as the number of molecules reacted per molecules of vanadium per unit time [23], the difference of the catalytic activity between the catalyst prepared in this study and that prepared by Quaranta et al. [21] can be judged by the comparison of temperature-dependent TOF for these two catalysts. As shown in Fig. 3, the reaction catalyzed by the catalyst prepared in this study

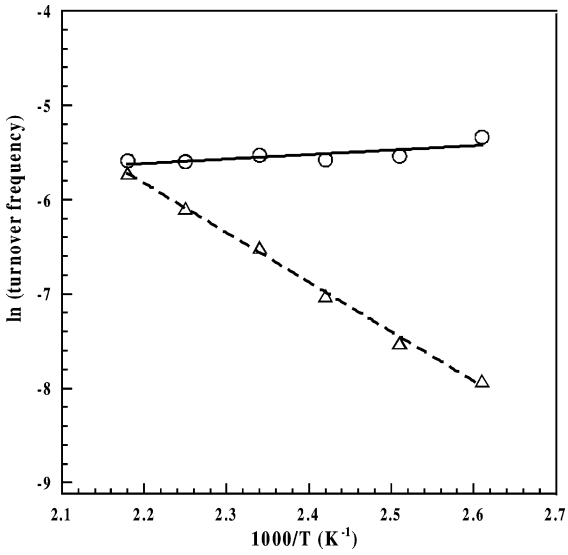

Fig. 3. Comparison of temperature dependence of TOF of ethanol oxidation catalyzed by the V_2O_5/TiO_2/MCM-41 catalyst prepared in this study (solid line) and the V_2O_5/2.0TiSi catalyst prepared by Quaranta et al. (dashed line).

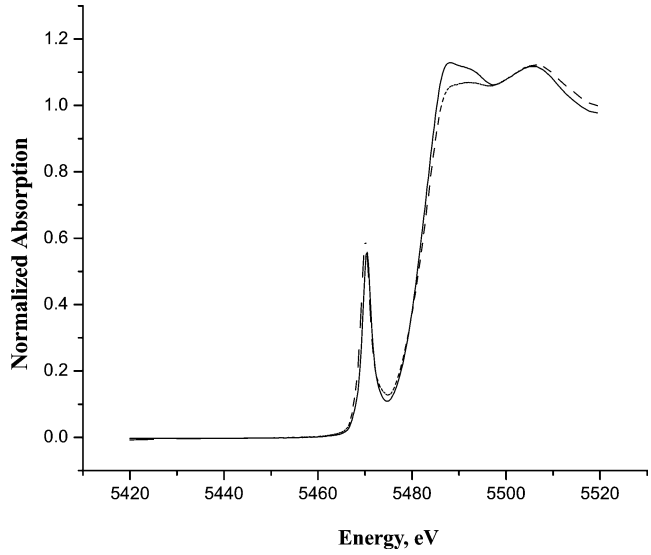

Fig. 4. V K-edge XANES spectra of V_2O_5/MCM-41 (solid line) and V_2O_5/TiO_2/MCM-41 (dashed line).

has an apparent activation energy of -6 kJ/mol, whereas the reaction catalyzed by the catalyst prepared by Quaranta et al. is about 46 kJ/mol. The difference of the catalytic properties for these two catalysts may be due to the difference of adsorption heat of ethanol caused by the interactions between V_2O_5 and TiO_2.

3.3. EXAFS and XANES analysis of vanadium

In order to elucidate the reason for the reactivity enhancement of V_2O_5 by TiO_2 in V_2O_5/TiO_2/MCM-41, EXAFS and XANES were used to characterize the vanadia on both supports. Normalized XANES spectra of V_2O_5/MCM-41 (solid line) and V_2O_5/TiO_2/MCM-41 (dash line) are shown in Fig. 4. It is generally accepted that the preedge peak found at the low energy side of the edge absorption reveals the coordination state of the vanadium complex [24]. It has been reported that the intensity of the preedged peak can be used to judge the coordination structure based on a detailed comparison of the V preedge peak intensities in different coordination environments [25,26]. Since we did not have reference XANES spectra of different coordination environments, it is difficult to judge the coordination environment of V by the intensity of the V preedge peak. However, we can hardly observe the characteristic bands of XANES (so called α and β band in Ref. [25]) which indicates that tetrahedral coordination environment contributes in the samples. In addition, the V preedged peak in the XANES spectra of our samples have intensities between the reported preedge peak intensities of tetrahedral VO_4 coordination structure and distorted VO_5 structure reported in the literature [26]. Based on these observations, we can not totally exclude the existence of tetrahedral VO_4 coordination structure or the distorted VO_5 structure. Since Debye–Waller factor and coordination number are highly correlated, different combinations of Debye–Waller factor and coordination number will give equal good fits of experimental data. However, according to the above discussion of XANES results, the average coordination number of V–O2 was fixed as 3.5 to decouple the correlation effects (Table 3).

The local structures around the vanadium atom of V_2O_5/MCM-41 (solid line) and V_2O_5/TiO_2/MCM-41 (dash line) became visually clearer when a Fourier transform was per-

Table 3
Structure parameters of the V_2O_5/MCM-41 and V_2O_5/TiO_2/MCM-41

Description	Scatterer	R (Å)	CN	$\Delta\sigma^2$	E_0 (eV)	EXAFS reference
V_2O_5/MCM-41	V–O1	1.603 ± 0.006	1.00[a]	0.0042 ± 0.0005	-8.02 ± 1.23	V–O
	V–O2	1.849 ± 0.005	3.50[a]	0.0126 ± 0.0004	-4.56 ± 0.64	V–O
	V–V	3.053 ± 0.006	1.31 ± 0.08	0.0086 ± 0.0009	-4.43 ± 0.52	V–V
V_2O_5/TiO_2/MCM-41	V–O1	1.595 ± 0.008	1.00[a]	0.0048 ± 0.0006	-7.66 ± 1.65	V–O
	V–O2	1.805 ± 0.008	3.50[a]	0.0153 ± 0.0008	-2.11 ± 1.11	V–O
	V–V	2.987 ± 0.018	1.29 ± 0.86	0.0036 ± 0.0040	5.53 ± 4.23	V–V
	V–Ti	2.868 ± 0.023	0.50 ± 0.41	0.0009 ± 0.0036	-6.37 ± 7.38	V–Ti

R, distance; CN, coordination number; $\Delta\sigma^2$, deviation of Debye–Waller factor; E/∂, inner-potential correction.
[a] The number of parameter used to fit the data.

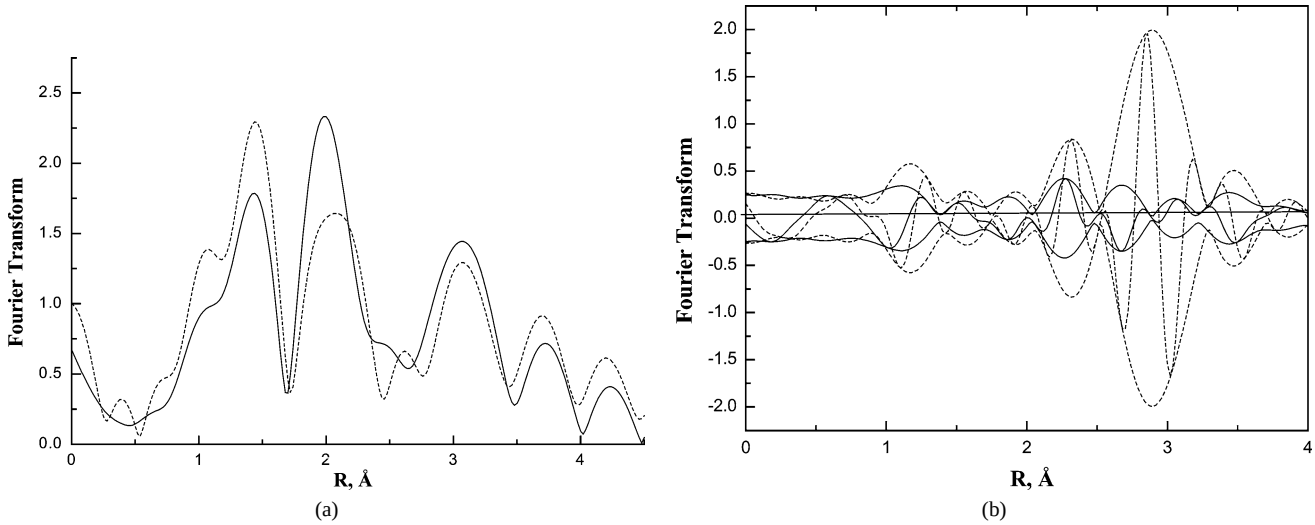

Fig. 5. (a) Fourier transform (k^3 weighted, V–O phase-corrected, $\Delta k = 3.5$–13.0 Å^{-1}) of raw EXAFS data for the V_2O_5/MCM-41 (solid line) and the V_2O_5/TiO_2/MCM-41 (dashed line). (b) Fourier transform (k^3 weighted, V–Ti phase-corrected, $\Delta k = 4.0$–14.0 Å^{-1}) of [raw data (V–O)–(V=O)–(V–O–V)] for V_2O_5/MCM-41 (solid line) and the V_2O_5/TiO_2/MCM-41 (dashed line).

formed on EXAFS in the 3.5–13.0 Å^{-1} region, to obtain the radial structure function as shown in Fig. 5a. In the V_2O_5/MCM-41 (solid line) sample, the two peaks appearing at 1.4 and 2.0 Å are assigned to V–O bonds. The third peak appearing at 3.0 Å may be caused by the presence of vanadium atoms adjacent to vanadium atoms (V–O–V), indicating the presence of neighboring vanadium atoms. In the V_2O_5/TiO_2/MCM-41 (dash line) sample, a similar pattern but with a lower intensity of the peak at 3.0 Å was observed. The weaker intensity of the peak suggests that the vanadium is better dispersed in V_2O_5/TiO_2/MCM-41. This is because the amounts of vanadia are similar in both samples; thus, less V–O–V contribution indicates the presence of a relatively small polymeric V_2O_5 size. Moreover, after subtracting two calculated V–O and V–O–V contributions from the raw data, a significant peak was observed only for the V_2O_5/TiO_2/MCM-41 sample. After V–Ti phase-corrected Fourier transform was performed on the resulting spectrum for the V_2O_5/TiO_2/MCM-41 sample, a symmetric peak was presented, suggesting that Ti is the backscattering atom (Fig. 5b). This observation suggests that V_2O_5 is anchoring on TiO_2 in the TiO_2/MCM-41 support and the interaction between V_2O_5 and TiO_2 retards the aggregation of V_2O_5 [27].

XANES spectra of V_2O_5/TiO_2/MCM-41 under hydrated and dehydrated conditions further support the direct interaction between V_2O_5 and TiO_2 in V_2O_5/TiO_2/MCM-41. It has been reported that hydration of TiO_2/SiO_2 decreases the preedge peak intensity and blue shifts the peak position in the XANES spectra compared to the XANES spectra of dehydrated TiO_2/SiO_2 [18,22]. This indicates that the coordination number of the Ti atoms increases mostly to 6-fold in the hydrated sample. In $V_2O_5/TiO_2/SiO_2$, coordination of V_2O_5 on TiO_2 resulted in a direct interaction with the surface titanium oxide species by binding to their unsaturated sites such that Ti cations are predominately 6-fold despite whether the sample is hydrated or dehydrated. The XANES spectra of hydrated and dehydrated V_2O_5/TiO_2/MCM-41 are similar, indicating that Ti cations in both samples are predominately 6-fold as shown in Fig. 6. This observation further implies the dispersion of V_2O_5 on TiO_2 in V_2O_5/TiO_2/MCM-41 [22].

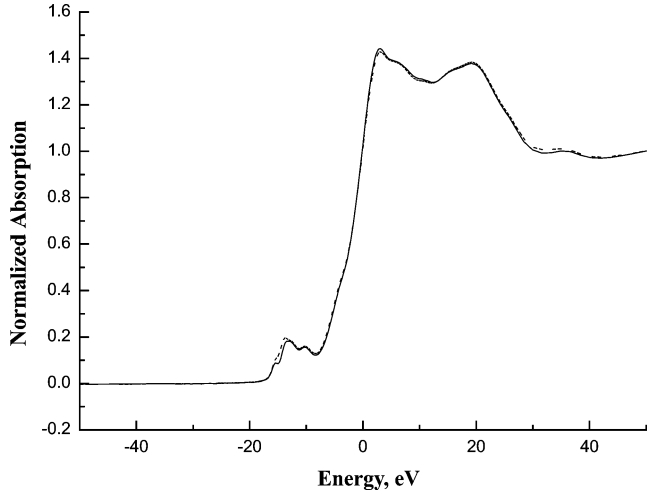

Fig. 6. Ti K-edge XANES spectra of the hydrated (solid line) and dehydrated (dashed line) V_2O_5/TiO_2/MCM-41 samples.

In summary, the EXAFS data are consistent with highly dispersed V on TiO_2 as shown by the presence of the V–O–Ti peak in the EXAFS of the V_2O_5/TiO_2/MCM-41 sample. This result is consistent with the reported UV-vis DRS study which indicates that the vanadium oxide species has a lower degree of polymerization on the dispersed TiO_2/SiO_2 support than on pure silica [22].

3.4. Catalytic properties and morphology of V_2O_5 on TiO_2/MCM-41

The morphologies of V_2O_5 are similar on both TiO_2/MCM-41 and MCM-41 since they are both polymeric. This indicates that the enhancement of the reactivity is not due to the different of morphologies of V_2O_5 on different supports. It has been reported that V_2O_5 has a higher reactivity on the TiO_2/SiO_2 support than on pure silica [15,16]. The basis for the reactivity enhancement of the isolated vanadia sites on TiO_2/SiO_2 supports has been extensively studied [22]. The enhancement of catalytic activity of V_2O_5 on TiO_2/SiO_2 is due to the coordination of V to Ti(IV) cations. The presence of V–O–Ti bonds was proposed to enhance the reactivity of the V active sites on the $V_2O_5/TiO_2/SiO_2$ catalyst [22].

As show in Fig. 3, the TOF for V_2O_5/TiO_2/MCM-41 catalysts is about 8 times that of $V_2O_5/TiO_2/SiO_2$ at 383 K whereas it is about the same when the reaction temperature was elevated to about 458 K. This turnover-frequency calculation is based on the total vanadium atom. For a heterogeneous catalytic reaction, the conversion is normally proportional to the surface atom. A catalyst with more surface atoms will present higher TOF. The surface area of V_2O_5/TiO_2/MCM-41 (700 m^2/g) is higher than that of $V_2O_5/TiO_2/SiO_2$ (70 m^2/g).

The fraction of V_2O_5 in contact with TiO_2 support is expected to be increased with increasing surface area. This increase in V_2O_5–TiO_2 contact may enhance the interactions between V_2O_5 and TiO_2 which further strengthen the affinity between ethanol and exposed V_2O_5. An increase of adsorption heat thus resulted. Since enthalpy of adsorption is almost negative, the apparent activation ($E_s + H_a$) will be decreased with the adsorption heat in the V_2O_5/TiO_2/MCM-41. Thus, the ethanol conversion is almost invariant to temperature. No such observation has been reported for $V_2O_5/TiO_2/SiO_2$ and V_2O_5/TiO_2/MCM-41. This interaction of V_2O_5 and TiO_2 is evidenced by the observation of the V–Ti EXAFS contribution at 2.8 Å in V_2O_5/TiO_2/MCM-41.

The apparent activation energy calculated for the low conversion range (reaction temperature less than 428 K) is about 46 kJ/mol for the V_2O_5/MCM-41 catalyst, and is similar to that for $V_2O_5/TiO_2/SiO_2$ and V_2O_5/SiO_2 catalysts reported by Quaranta et al. [21]. Further elevation of reaction temperature promotes the conversion of acetaldehyde and acetic acid to carbon dioxide (Table 2). Since ethanol conversion and the formation of carbon dioxide from acetaldehyde and acetic acid may take place at the same active sites, sites for ethanol conversion decrease with increasing carbon dioxide formation. As shown in Fig. 2 and Table 2, as the temperature increases from 428 to 458 K, the ethanol conversion is only slightly increased, whereas the carbon dioxide yield increases abruptly from 0.110 wt% of product to 0.372 wt% for V_2O_5/MCM-41 catalysts.

Better dispersion of V_2O_5 on the support due to the interaction between V_2O_5 and TiO_2 thus provides more active sites for the oxidation reaction. As a result, at a low temperature (383 K), much higher activity was observed for V_2O_5/TiO_2/MCM-41. On the other hand, enthalpy of adsorption is increased by the interaction between V_2O_5 and TiO_2, leading to a decline of apparent activation energy. As a result, the activity of the catalysts cannot be enhanced by the elevation of reaction temperature at this temperature range.

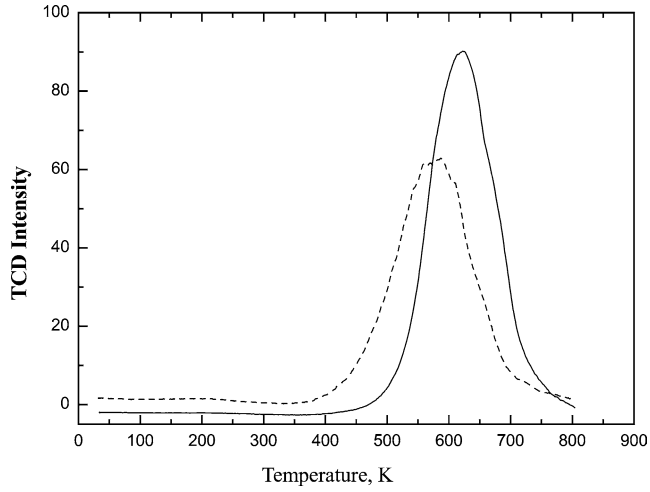

Fig. 7. Temperature-programmed reduction characterizing V_2O_5/MCM-41 (solid line) and V_2O_5/TiO_2/MCM-41 samples (dashed line).

The selectivity of the catalysts is also influenced by the interaction between V_2O_5 and TiO_2. At a reaction temperature of 383 K, for V_2O_5/TiO_2/MCM-41, the major product is acetaldehyde (0.732 mol fraction). Acetic acid only exists in a trace amount. For V_2O_5/MCM-41, only 0.466 mol fraction is acetaldehyde and 0.196 mol fraction is acetic acid. When the temperature is raised to 458 K, acetaldehyde is still a major product for V_2O_5/TiO_2/MCM-41. However, carbon dioxide (0.372 mol fraction) is the major product for V_2O_5/MCM-41.

TPR profiles of V_2O_5/TiO_2/MCM-41 and V_2O_5/MCM-41 show that the reduction temperatures of these two catalysts are different (Fig. 7). The T_{max} value of V_2O_5/TiO_2/MCM-41 is about 50 K lower than the T_{max} value of V_2O_5/MCM-41, indicating the polymeric V_2O_5 exhibits a higher reducibility in V_2O_5/TiO_2/MCM-41 than in V_2O_5/MCM-41. This is consistent with the reported higher reducibility of V_2O_5 in $V_2O_5/TiO_2/SiO_2$ compared to that in V_2O_5/SiO_2 when the sample has high V_2O_5 and TiO_2 loadings [22]. Although, we do not have direct evidence that V_2O_5 on TiO_2/MCM-41 is totally dispersed on TiO_2, EXAFS analysis of $V_2O_5/TiO_2/SiO_2$ at the V K-edge and Ti K-edged XANES spectra of V_2O_5/TiO_2/MCM-41 under hydrated and dehydrated conditions, enhancement of reactivity toward the oxidation of ethanol, different reactivity and selectivity at elevated temperatures, and different morphologies on the two different supports indirectly indicate V_2O_5 is at least partially if not all coordinated to TiO_2 in V_2O_5/TiO_2/MCM-41.

4. Conclusions

This report demonstrates that TiO_2-grafted MCM-41 can be used as a support for vanadia-based catalysts. The resultant V_2O_5/TiO_2/MCM-41 has better catalytic reactivity than V_2O_5/MCM-41 toward the oxidation of ethanol. This reactivity enhancement is consistent with the reported reactivity enhancement of $V_2O_5/TiO_2/SiO_2$ compared with V_2O_5/SiO_2 toward the same catalytic oxidation reaction [21,22]. Thus, this TiO_2-grafted MCM-41 mesoporous framework has high potential for use as a mesoporous TiO_2 support with higher surface area for other catalysts. Such support is superior to traditional anatase TiO_2, pure mesoporous TiO_2, or TiO_2/SiO_2 supports owing to its much larger surface area and better thermal stability at elevated temperatures.

Acknowledgments

The EXAFS data were analyzed using the XDAP Data Analysis Program, developed by M. Vaarkamp, J.C. Linders, and D.C. Koningsberger, and the reference files were provided by Dr. B.C. Gates. We also acknowledge support from Academia Sinica, Synchrotron Radiation Research Center (SRRC), and National Science Council, Taiwan, ROC.

References

[1] K.I. Hadjiivanov, D.G. Klissurski, Chem. Soc. Rev. 25 (1996) 61.
[2] M.A. Reiche, E. Ortelli, A. Baiker, Appl. Catal. B 23 (1999) 187.
[3] V.M. Mastikhin, V.V. Terskikh, O.B. Lapina, S.V. Filimonova, M. Seidl, H. Knözinger, J. Catal. 156 (1995) 1.
[4] J.S. Beck, J.C. Vartuli, W.J. Roth, M.E. Leonowicz, C.T. Kresge, K.D. Schmitt, C.T.-W. Chu, D.H. Olson, E.W. Sheppard, S.B. McCullen, J.B. Higgins, J.L. Schlenker, J. Am. Chem. Soc. 114 (1992) 10834.
[5] V.F. Stone Jr., R.J. Davis, Chem. Mater. 10 (1998) 1468.
[6] P. Yang, D. Zhao, D.I. Margolese, B.F. Chmelka, G.D. Stucky, Nature 396 (1998) 152.
[7] D.M. Antonelli, J.Y. Ying, Angew. Chem. Int. Ed. Engl. 34 (1995) 2014.
[8] D.J. Jones, G. Aptel, M. Brandhorst, M. Jacquin, J. Jiménez-Jiménez, A. Jiménez-López, P. Maireles-Torres, I. Piwonski, E. Rodríguez-Castellón, J. Zajac, J. Rozière, J. Mater. Chem. 10 (2000) 1957.
[9] H. Yoshitake, T. Slugihara, T. Tatsumi, Chem. Mater. 14 (2002) 1023.
[10] D.M. Antonelli, Micropor. Mesopor. Mater. 30 (1999) 315.
[11] T. Maschmeyer, F. Rey, G. Sankar, J.M. Thomas, Nature 378 (1995) 159.
[12] M.S. Morey, S. O'Brien, S. Schwarz, G.D. Stucky, Chem. Mater. 12 (2000) 898.
[13] M. Vaarkamp, J.C. Linders, D.C. Koningsberger, Phys. B 209 (1995) 159.
[14] M. Vaarkamp, I. Dring, R.J. Oldman, E.A. Stern, D.C. Koningsberger, Phys. Rev. B 50 (1994) 7872.
[15] J.W. Cook Jr., D.E. Sayers, J. Appl. Phys. 52 (1981) 5024.
[16] J.B.A.D. van Zon, D.C. Koningsberger, H.F.J. van 't Blik, D.E. Sayers, J. Chem. Phys. 82 (1985) 5742.
[17] S.I. Zabinsky, J.J. Rehr, A. Ankudinov, R.C. Albers, M.J. Eller, Phys. Rev. B 52 (1995) 2995.
[18] X. Gao, S.R. Bare, J.L.G. Fierro, M.A. Banares, I.E. Wachs, J. Phys. Chem. B 102 (1998) 5653.
[19] C.-F. Cheng, K.H. Park, J. Klinowski, J. Chem. Soc., Faraday Trans. 93 (1997) 193.
[20] C.R. Dias, M.F. Portela, G.C. Bond, J. Catal. 157 (1995) 344.
[21] N.E. Quaranta, J. Soria, V. Cortes Corberan, J.L.G. Fierro, J. Catal. 171 (1997) 1.
[22] X. Gao, S.R. Bare, J.L.G. Fierro, I.E. Wachs, J. Phys. Chem. B 103 (1999) 618.
[23] J.M. Thomas, W.J. Thomas, Principles and Practice of Heterogeneous Catalysis, VCH, Weinheim, 1997.
[24] A. Bianconi, in: D.C. Koningsberger, R. Prins (Eds.), X-Ray Absorption—Principles, Applications, Techniques of EXAFS, SEXAFS, and XANES, Wiley, New York, 1988, p. 573.
[25] S.G. Zhang, S. Higashimoto, H. Yamashita, M. Anpo, J. Phys. Chem. B 102 (1998) 5590.
[26] T. Tanaka, H. Yamashita, R. Tsuchitani, T. Funabiki, S. Yoshida, J. Chem. Soc., Faraday Trans. 1 84 (1988) 2987.
[27] C.B. Wang, Y. Cai, I.E. Wachs, Langmuir 15 (1999) 1223.